water

MDPI

Article

Suitability of UAV-Based RGB and Multispectral Photogrammetry for Riverbed Topography in Hydrodynamic Modelling

Vytautas Akstinas [1,*], Karolina Gurjazkaitė [1], Diana Meilutytė-Lukauskienė [1], Andrius Kriščiūnas [2], Dalia Čalnerytė [2] and Rimantas Barauskas [2]

[1] Laboratory of Hydrology, Lithuanian Energy Institute, Breslaujos St. 3, LT-44403 Kaunas, Lithuania
[2] Department of Applied Informatics, Kaunas University of Technology, Studentų St. 50, LT-51368 Kaunas, Lithuania
* Correspondence: vytautas.akstinas@lei.lt

Abstract

This study assesses the suitability of UAV aerial imagery-based photogrammetry for reconstructing underwater riverbed topography and its application in two-dimensional (2D) hydrodynamic modelling, with a particular focus on comparing RGB, multispectral, and fused RGB–multispectral imagery. Four Lithuanian rivers—Verknė, Šušvė, Jūra, and Mūša—were selected to represent a wide range of hydromorphological and hydraulic conditions, including variations in bed texture, vegetation cover, and channel complexity. High-resolution digital elevation models (DEMs) were generated from field-based surveys and UAV imagery processed using Structure-from-Motion photogrammetry. Two-dimensional hydrodynamic models were created and calibrated in HEC-RAS 6.5 using measurement-based DEMs and subsequently applied using photogrammetry-derived DEMs to isolate the influence of terrain input on model performance. The results showed that UAV-derived DEMs systematically overestimate riverbed elevation, particularly in deeper or vegetated sections, resulting in underestimated water depths. RGB imagery provided greater spatial detail but was more susceptible to local anomalies, whereas multispectral imagery produced smoother surfaces with a stronger positive elevation bias. The fusion of RGB and multispectral imagery consistently reduced spatial noise and improved hydrodynamic simulation performance across all river types. Despite moderate vertical deviations of 0.10–0.25 m, relative flow patterns and velocity distributions were reproduced with acceptable accuracy. The findings demonstrate that combined spectral UAV aerial imagery in photogrammetry is a robust and cost-effective alternative for hydrodynamic modelling in shallow lowland rivers, particularly where relative hydraulic characteristics are of primary interest.

Keywords: UAV photogrammetry; riverbed topography; digital elevation model (DEM); hydrodynamic modelling; HEC-RAS; bathymetry accuracy; fluvial morphology

Academic Editor: Salvatore Ivo Giano

Received: 23 November 2025
Revised: 16 December 2025
Accepted: 19 December 2025
Published: 22 December 2025

1. Introduction

Hydrodynamic models play a crucial role in river engineering, catchment planning, and flood risk management. These models provide important insights into flow dynamics, sediment transport, and energy distribution, and serve as decision-making tools for infrastructure development, ecological planning, and climate adaptation strategies [1,2].

However, the performance of such models depends heavily on the quality of the topographic input data, particularly Digital Elevation Models (DEMs), which must accurately capture terrestrial, subsurface, and inundated features of the riverbed.

Numerous studies have shown that inaccuracies in DEMs can propagate through hydraulic simulations and significantly affect predictions, including water surface elevation, flood extent, and velocity distributions [3,4]. Recent efforts in ensemble-based flood risk modelling have also confirmed that uncertainties associated with DEMs affect the reliability of spatial flood predictions and the delineation of protection zones [5]. Even small errors in bathymetric inputs, especially in shallow, vegetated, or morphologically complex river reaches, can cause significant deviations in modelled results, particularly in low-energy river systems and floodplains.

To address these limitations, researchers have adopted UAV imagery-based photogrammetry and structure-from-motion (SfM) techniques as cost-effective alternatives for capturing high-resolution channel morphology or riverbed topography. Several recent studies, including the integration of UAV surface velocimetry and photogrammetry, have shown promising results in medium and large rivers, achieving improved bathymetry data [6,7]. The "Fluvial Domain Method" and other structure-from-motion approaches demonstrate the feasibility of generating DEMs from UAV imagery in data-poor or inaccessible regions [8]. However, the robustness of these methods under varying geomorphological and hydrological conditions remains insufficiently validated, particularly for smaller and ecologically complex river systems in Central and Eastern Europe.

Photogrammetry using overlapping UAV imagery enables the production of detailed topographic and bathymetric DEMs under favorable environmental conditions, such as clear water, minimal vegetation, and stable illumination [9]. Its advantages include reduced on-site logistics, lower costs, and high spatial resolution. However, photogrammetric performance is strongly affected by water clarity, surface reflectance, aquatic vegetation, and turbidity, which contribute to depth-dependent vertical uncertainty in reconstructing DEMs [10–12]. Previous studies have highlighted the increasing robustness of UAV-derived DEMs in hydraulic modelling applications. Hawker [13] demonstrated shallow river bathymetry with acceptable errors, while Langhammer et al. [14] successfully integrated UAV-derived topography into 2D flood modelling. Annis et al. [15] found that UAV-based DEMs compare well with LiDAR for small-scale flood hazard mapping, and Masafu et al. [16] validated UAV-based velocity measurements with acoustic Doppler data, achieving error margins of approximately 4.2%. Further developments, including machine learning-based refraction corrections [17,18] and UAV–USV sensor fusion [19], continue to expand the applicability of photogrammetry in aquatic environments.

Despite these advantages, obtaining reliable bathymetric data remains challenging, particularly in shallow, vegetated, or inaccessible river sections. Conventional survey methods, such as boat-mounted echosounders, total stations, and terrestrial laser scanning, are generally the most accurate but are logistically challenging, costly, and often unsuitable for turbulent or vegetated environments [20–22]. Additionally, DEMS interpolation methods can introduce further uncertainty, with the choice of method influencing the final terrain representation [23]. Comprehensive evaluations of UAV-derived DEMs for hydrodynamic modelling across different river environments are still lacking. Song et al. [4] found good agreement between corrected UAV-derived and field-based topography data, with relative errors of 0.17 m, and improved interpolation accuracy by 55% using a dimensionless channel width correction. Meanwhile, hybrid and data-driven bathymetric models are also emerging. Bures et al. [24] presented the Bathy-Supp model, a statistically parameterized approach that outperformed traditional DEM inputs in HEC-RAS simulations. These studies show that empirical and remote sensing-based bathymetric models are advancing

rapidly, but comparative assessments on geomorphologically variable rivers remain scarce in scientific studies. Importantly, most existing UAV-based bathymetry studies rely primarily on RGB imagery or focus on dry or partially inundated floodplains [12,25]. Few studies have systematically examined how different spectral inputs (such as RGB and multispectral imagery) and their combination influence photogrammetric DEM quality [26,27]; however, the studies lack the analysis of how these differences propagate into hydrodynamic model performance. Comparative assessments across rivers with contrasting bed texture, vegetation cover, and morphological complexity are still scarce.

In this context, the present study aims to assess the suitability of UAV-derived DEMs for hydrodynamic modelling in four Lithuanian rivers: Verknė, Šušvė, Jūra, and Mūša. These rivers represent a range of hydromorphological conditions, including sandy and gravel beds, boulder-dominated reaches, and sections with varying degrees of aquatic vegetation. High-resolution DEMs were generated from on-site surveys and UAV imagery using RGB-only, multispectral-only, and fused RGB–multispectral photogrammetry. These DEMs were then integrated into two-dimensional hydrodynamic models developed in HEC-RAS 6.5 and calibrated against observed water levels and measured flow velocities. The objectives of this study are to (i) quantify elevation errors associated with different spectral photogrammetry inputs, (ii) evaluate how RGB, multispectral, and fused DEMs influence hydrodynamic simulation results, and (iii) identify river conditions under which spectral fusion provides added value. Unlike previous studies that primarily assess bathymetric accuracy, this work explicitly examines how the choice of spectral input propagates into hydrodynamic model performance across rivers with contrasting bed texture, vegetation, and morphological complexity.

2. Study Area, Data and Methods

2.1. Study Area

This study was conducted on selected stretches of four Lithuanian rivers: Verknė, Šušvė, Jūra, and Mūša. These rivers were chosen to represent a wide range of hydromorphological and hydraulic conditions in different hydrological regions of the country (Figure 1).

Lithuania has a humid mid-latitude transitional climate, ranging from maritime to continental, with an average annual temperature of 7.4 °C and annual precipitation of around 695 mm, according to the Lithuanian Hydrometeorological Service. These climatic conditions support year-round river runoff, with discharge peaks typically in spring. All river stretches had relatively natural morphology and low anthropogenic impact on river morphology, although hydropower plants were present upstream of selected sites. All sites were fully wadable for field measurements under low- to moderate-flow conditions. The selected river sections included channels with varying morphologies, from shallow, vegetated streams dominated by fine sediments to deeply incised gravel and boulder channels, making them ideal case studies for evaluating the performance of UAV imagery-based photogrammetry under different environmental conditions. To support analysis of how environmental and physical conditions affect photogrammetric performance, we summarized key fluvio-geomorphic properties of each study stretch in Table 1.

Table 1. Physical properties of selected river stretches, ordered according to their complexity.

River	Stretch Length (m)	Channel Width (m)	Mean Depth (m)	Maximum Depth (m)	Substrate	Vegetation Type	Measurement Points
Šušvė	35	8–11	0.26	0.40	Sand, gravel, cobble	Sparse algae	238
Jūra	134	12–20	0.34	0.89	Gravel, cobble, boulders	No vegetation	305

Table 1. *Cont.*

River	Stretch Length (m)	Channel Width (m)	Mean Depth (m)	Maximum Depth (m)	Substrate	Vegetation Type	Measurement Points
Verknė	198	16–19	0.47	1.77	Sand, gravel, cobble	Dense aquatic vegetation	338
Mūša	338	7–22	0.28	1.02	Sand, cobble, boulders	Moderate aquatic vegetation	473

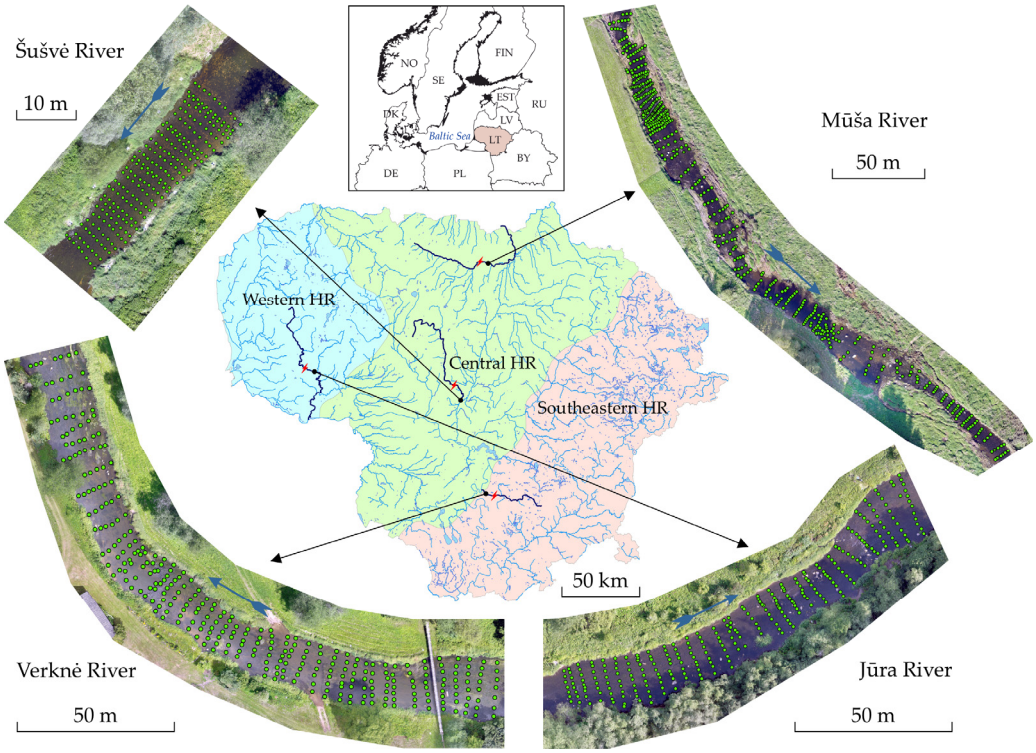

Figure 1. Study area and locations of the study sites on four Lithuanian rivers (Šušvė, Verknė, Jūra, and Mūša), measurement points (green dots), flow direction (blue arrows) and upstream hydropower plants (red thunderbolts).

2.2. Field Data Collection

Field data were collected to generate high-resolution topographic and bathymetric data along each stretch of the selected rivers and to support validation of UAV-derived digital elevation models (DEMs). Riverbed elevation data were collected using a high-precision GeoMax Zenith 40 GNSS receiver (GeoMax AG, Widnau, Switzerland) paired with a handheld tablet and X-PAD Ultimate Survey (version 24.5.1) software, providing horizontal and vertical accuracy of ±0.015 m. All surveyed reaches were fully wadable, allowing the operator to move across the riverbed with a handheld GNSS pole and manually record submerged points. Each site included 238–473 elevation points located both across the channel width and along the flow path, ensuring high spatial coverage of morphological variability (Figure 1). These points served as an independent validation dataset to assess the accuracy of the photogrammetry-based DEMs.

Additionally, water surface elevations were measured under two different discharge conditions for each river (a low-flow and a moderate-flow scenario) to calibrate and validate the hydrodynamic model. At each point where elevation was recorded, flow velocity was measured at 0.6 of the depth to represent depth-averaged flow velocity using a Valeport Model 801 electromagnetic flow meter. This sensor is well-suited to vegetated environments due to its robust, non-mechanical design.

Field-based bathymetric surveys and UAV image acquisition were carried out during the same field campaign under stable flow conditions of the same discharge. The time lag between UAV flights and in situ measurements did not exceed several hours. Although this short delay minimizes the likelihood of significant water-level changes, minor bed surface adjustments cannot be fully excluded and may contribute to small local elevation variability.

2.3. UAV Image Acquisition

RGB and multispectral aerial imagery were captured simultaneously using a DJI Mavic 3 Multispectral UAV (DJI, Shenzhen, China) equipped with an RTK positioning module. The drone features a 4/3-inch RGB CMOS sensor (3840 × 2160 px) and a 1/2.8-inch multispectral CMOS sensor (2592 × 1944 px) with four spectral bands: green (560 ± 16 nm), red (650 ± 16 nm), red edge (730 ± 16 nm), and near-infrared (860 ± 26 nm). All flights were conducted at a height of 30 m above the surface, except over the Jūra River, where the flight height was 40 m to avoid tall trees. An 80% forward overlap and a 75% side overlap between images were used to ensure complete stereoscopic coverage and optimal input for Structure-from-Motion (SfM) processing. These flight conditions ensured a ground sampling distance (GSD) of approximately 0.010 m for RGB and 0.018 m for multispectral bands. For precise georeferencing of aerial imagery, ten ground control points (GCPs) were measured per site using the same GNSS equipment. These GCPs were used exclusively for calibration of the photogrammetric outputs (orthomosaics and DEMs) and were not included in the validation process. DEM accuracy was independently assessed using only the in situ GNSS point measurements.

2.4. DEM Generation and Spectral Variants

Photogrammetric processing was carried out in Pix4Dmapper (version 4.9.0) using standard Structure-from-Motion (SfM) workflows. Key point detection and tie-point alignment were applied to overlapping aerial images to generate dense point clouds. Ground control points (GCPs) were manually identified in the imagery and used for accurate georeferencing and vertical calibration, minimizing geometric distortions.

Three sets of DEMs were produced for each river stretch: (i) DEMs derived from RGB imagery only, (ii) DEMs derived from multispectral imagery only, and (iii) DEMs derived from fused RGB–multispectral datasets. RGB and multispectral images were first processed separately to generate spectrum-specific DEMs. For the fused dataset, all available RGB and multispectral images were processed together within a single Pix4Dmapper project as a joint input dataset.

No manual resampling or prior unification of spatial resolution was applied to the RGB or multispectral imagery before fusion towards key point extraction. Differences in native image resolution and sensor characteristics were handled internally by Pix4Dmapper during the SfM and multi-view stereo processing stages, since the DEM output was rougher than GSD of multispectral band or even RGB. All RGB and multispectral images were included with equal priority, and no predefined weighting or proportions were assigned to either spectrum type. This means all input bands contributed equally to the key point extraction rather than one being dominant over another by default. The resulting fused DEM therefore represents an integrated surface reconstructed from all spectral inputs.

DEMs were generated from ground-classified dense point clouds using Inverse Distance Weighting (IDW) interpolation and exported at a spatial resolution finer than 0.1 m for subsequent analysis. No corrections for underwater light refraction were applied; this methodological limitation is addressed in the Section 4.

2.5. Hydrodynamic Modelling

Two-dimensional hydrodynamic simulations were carried out using HEC-RAS version 6.5. A reference model was created for each case study stretch based on the DEM derived from field measurements and calibrated using observed water surface elevations and flow velocity fields at known discharges (2.11 m^3/s in Verknė, 0.7 m^3/s in Šušvė, 1.01 m^3/s in Jūra, and 0.5 m^3/s in Mūša). All models used a 0.5 × 0.5 m mesh grid, except for the Šušvė River, which used a 0.25 × 0.25 m mesh grid, as this relatively simple case served as a reference to test hydrodynamic modelling performance under near-ideal natural conditions. Calibration parameters included Manning's roughness coefficient, energy grade line slope, and inflow and outflow boundary conditions. Manning's roughness coefficients were initially estimated considering the target channel substrate, vegetation, and slope. These values were iteratively calibrated to minimize the difference between modelled and measured water surface elevations and average flow velocities, ensuring a balance between positive and negative deviations of flow velocity. The final roughness values were selected based on achieving less than 0.005 m deviation in water surface elevation and less than 5% difference in average flow velocity. Validation was performed using the average water level height along the river stretch at known discharge. After successful calibration, the photogrammetry-derived DEMs (RGB, multispectral, and their fusion) were integrated into the same HEC-RAS models, with all other model parameters held constant. This enabled an isolated assessment of how the terrain, based solely on different aerial image input sources, may affect the hydrodynamic simulation results.

3. Results

3.1. Photogrammetry-Based Riverbed Topography

Photogrammetric reconstruction of riverbed topography using UAV imagery revealed consistent spatial patterns of depth deviations in the four case study rivers: Šušvė, Jūra, Verknė, and Mūša (Figure 2). In general, photogrammetry-based digital elevation models (DEMs) tended to overestimate riverbed elevation, especially in deeper or vegetated zones, resulting in underestimation of water depths compared to field observations. This pattern was observed across all analyzed river stretches, causing root mean square errors (RMSE) and mean absolute errors (MAE) of depth to range from 0.094 in shallow stretches to 0.207 in deeper, highly vegetated stretches (Table 2).

Table 2. Summary of depth RMSE (m) and MAE (m) for each spectrum-based DEM compared with observation points at selected river sites.

Spectrum	Metric	Šušvė	Jūra	Verknė	Mūša
RGB	RMSE	0.099	0.131	0.143	0.181
	MAE	0.094	0.106	0.115	0.134
Multispectral	RMSE	0.125	0.149	0.207	0.192
	MAE	0.119	0.109	0.157	0.159
Multispectral+RGB	RMSE	0.115	0.150	0.191	0.204
	MAE	0.111	0.119	0.168	0.180

Additionally, there was an anomaly zone where depth was greatly overestimated, reaching several times the actual depth (Figure 2). This tendency was found for all imagery spectra and indicated a systematic bias due to shading and other incorrect optical interpretations of surface location in the 3D environment. Such anomalies were found only with RGB imagery in the Verknė and Mūša rivers and were also reflected in the RGB with multispectral combination.

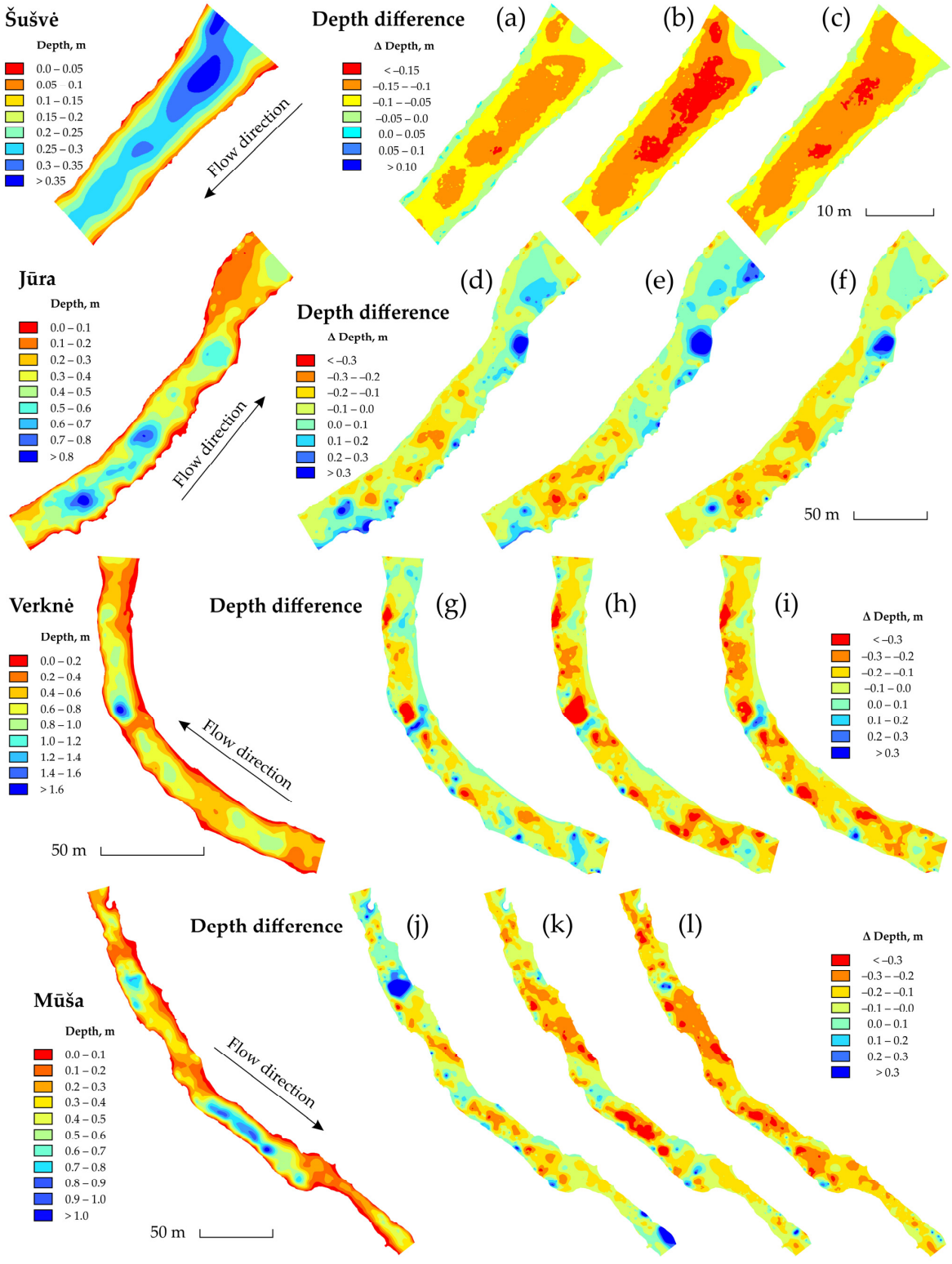

Figure 2. Bathymetry based on field measurements and photogrammetry-based depth differences compared to real observations (Δ Depth, m) in case study rivers using (**a**,**d**,**g**,**j**) RGB, (**b**,**e**,**h**,**k**) multispectral, and (**c**,**f**,**i**,**l**) RGB combined with multispectral images.

DEMs derived from RGB showed the smallest absolute mean vertical deviations but exhibited greater spatial variability and local anomalies, as previously mentioned (Figure 2a,d,g,j). This may be due to insufficient interpretation of the depth map in the RGB spectrum and its sensitivity to environmental factors. Multispectral DEMs provided smoother spatial patterns with fewer opposite-sign depth deviations but tended to over-

estimate depths more consistently throughout the channel (Figure 2b,e,h,k). The use of multispectral images in the photogrammetry process resulted in an overall increase in underwater topography but also captured relative depth distribution more accurately, indicating more precise determination of relative differences and improved depth interpretation.

The fusion of RGB and multispectral images produced the most balanced results for spatial noise, although absolute vertical deviations in depth were still underestimated, with average depth 0.1–0.2 m lower than observed values (Figure 2c,f,i,l). Strong anomaly zones of depth overestimation persisted and were influenced by the RGB imagery, indicating that the impact of this spectrum remained proportionally strong and involved not only improvements but also the transfer of related anomalies. The performance of separate and combined spectra in the photogrammetry process varied depending on morphology diversity and the presence of boulders at study sites. The largest deviations occurred in the densely vegetated sections of the Verknė and Mūša rivers, while strong depth anomaly zones were observed in sections with abundant boulders.

Based on depth anomalies, the main source of differences was the overestimation or underestimation of underwater elevation, which played a crucial role across the study sites. Therefore, a two-part analysis of underwater elevation deviations between the DEMs derived from the UAV and the riverbed heights measured in the field was carried out in the analyzed river stretches (Figure 3). The histograms showed the distributions of photogrammetry-based elevation differences from the observed values within specific intervals, while the relation plots illustrated the relationship between the elevation deviations and the actual measured depth to indicate the influence of river depth on potential deviation of underwater elevation. All analyzed data for the four rivers were spatially discretized into regular grid cells corresponding to the HEC-RAS 2D grid resolution (0.25×0.25 m for Šušvė and 0.5×0.5 m for the other rivers, i.e., Jūra, Verknė and Mūša). The histograms represented the number of cells falling within certain elevation deviation intervals. In addition to vegetation cover and coarse substrate elements, increased scatter in elevation differences was observed in river sections with gravel or mixed-bed material. These sections showed greater variability in photogrammetry-derived elevations compared to field measurements, particularly in shallow areas. Although sediment transport was not measured directly, the observed variability suggests that short-term changes in the riverbed surface may contribute to elevation scatter in fine-grained substrates.

Positive values indicate an overestimation of the riverbed elevation (i.e., an underestimation of the river depth), and negative values indicate an underestimation of the height. The Šušvė River, which is morphologically simple and shallow, showed systematic positive elevation deviations in all image types. RGB, multispectral, and combined datasets all produced DEMs that overestimated elevation by 0.06 to 0.16 m, indicating uniform overestimation due to refraction and minimal vegetation interference. In Jūra, characterized by clean water and abundant boulders, the RGB-derived DEMs mostly overestimated elevations by 0–0.2 m, while the multispectral data captured a wider distribution (-0.1 to $+0.1$ m), indicating increased vertical variability. The fusion of RGB and multispectral data reduced negative outliers but concentrated elevation estimates within the interval of 0.05 to 0.15 m higher than the observed values. The tendencies in the Verknė River, with high aquatic vegetation cover, reflected the previous river in RGB terms but showed a strong positive bias for the multispectral DEMs, with a peak concentration in the 0.1–0.15 m interval. The combination of image spectra did not reduce this overestimation but narrowed the distribution, indicating improved consistency but persistent bias.

The Mūša River, a structurally complex river with vegetation and boulders, showed clear discrepancies between RGB and multispectral results. RGB DEMs showed positive deviations concentrated between 0 and 0.15 m, while multispectral data showed an in-

creased overestimate by an additional 0.05 m. Merging both spectra reduced the relative spread of deviations across the segment but increased the absolute elevation of the selected river stretch. This tendency centered the results of deviations at around 0.1–0.25 m higher elevation than the observed values. These histograms confirm that while RGB imagery offers high spatial resolution, it is more prone to underestimation in optically complex environments. Conversely, multispectral imagery showed a stronger positive absolute bias, especially in highly vegetated river stretches. Meanwhile, the fusion of applied imagery spectra consistently increased the average deviations of the selected river stretches.

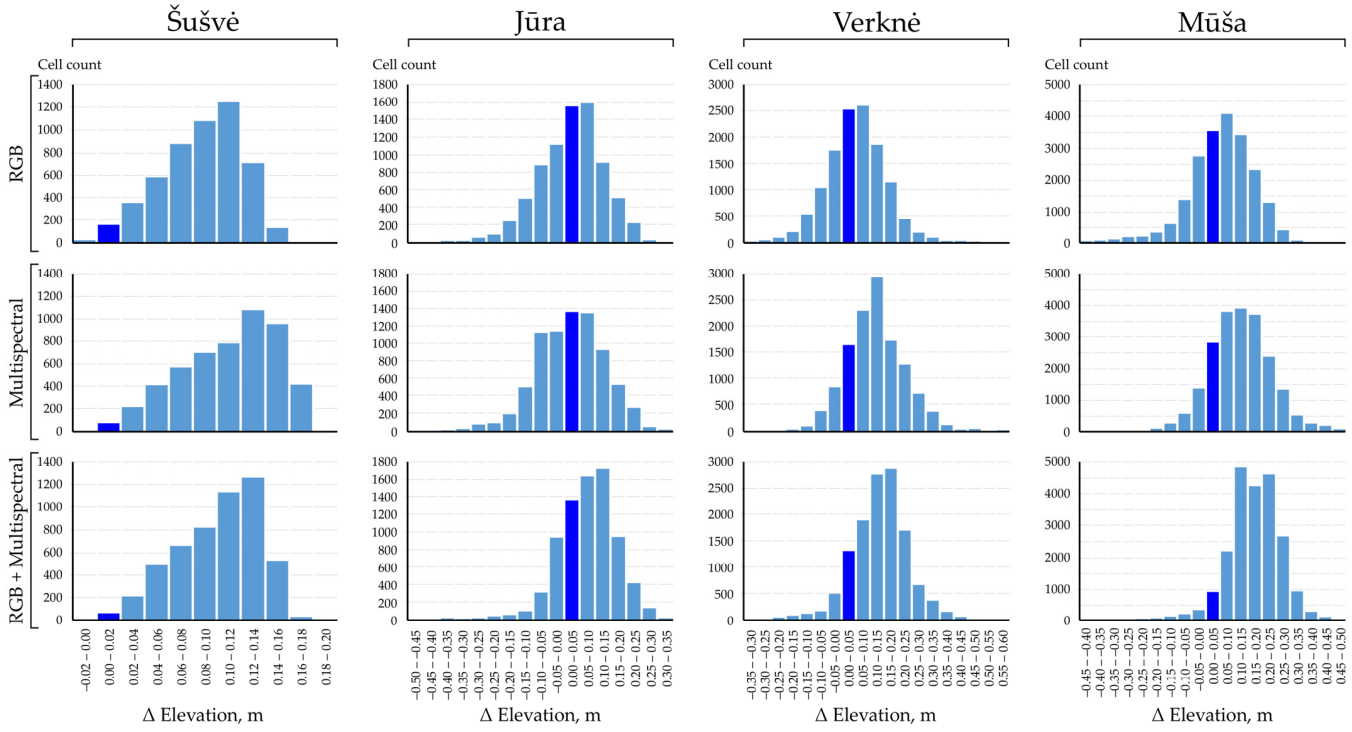

Figure 3. Distribution of riverbed topography differences between photogrammetry-based DEM (RGB, multispectral, and RGB with multispectral imagery) and observed elevation (dark blue column indicating the first interval of positive deviations) in the Šušvė, Jūra, Verknė, and Mūša rivers.

The dependence of underwater elevation deviations on river depth was also analyzed (Figure 4). In the Šušvė River, evaluation of deviations showed a positive relation with depth. An average deviation of +0.1 m was recorded at a depth of 0.3 m, indicating a refraction-induced vertical distortion consistent across all image types. However, the combination of RGB and multispectral images produced less scattered results and a more clearly expressed relation. In the Jūra River, deviation patterns were more homogeneous. Regardless of the selected imagery, all combinations showed a tendency for increasing deviations with increasing depth. The presence of deep negative deviations of underwater elevation indicated local anomalies possibly related to reflectance confusion from environmental distortions, but these were not related to depth. The Verknė River, with abundant aquatic vegetation, showed a strong positive dependence of elevation deviations on depth, especially for multispectral imagery. Here, overestimations of underwater elevation increased with depth, reaching +0.2 m for every 0.2 m of depth below 1 m. In contrast, RGB imagery showed only a +0.05 m increase in elevation for the same depth conditions. The combination of RGB and multispectral images reduced both the magnitude and slope of elevation deviation for depths below 1 m, indicating attenuation of depth-related distortion. In the most complex stretch of the Mūša River, the RGB-derived DEMs exhibited negative deviation anomalies similar to those in the Jūra, but the Mūša was distinguished by

two zones of such divergence. The multispectral results significantly improved the generation of underwater elevation compared to RGB, but the tendency for increasing deviations with depth was also observed. Fusion of image spectra suppressed extreme values and reduced the overall relationship, resulting in more stable elevation estimates at depths greater than 0.6 m. These tendencies suggest that depth-dependent elevation biases are a persistent feature of UAV imagery-based photogrammetry, caused by optical distortions such as light refraction, water surface reflection, and subsurface signal scattering. While RGB imagery captures underwater elevation well in shallow, clear conditions, it tends to underestimate relative elevation differences. Multispectral imagery offers more stable detection in changing light conditions and instream environments but often smooths out topographical details and overestimates the absolute height of underwater elevation. The combination of both sensors compensates for these effects and provides higher reliability for topographic data in further applications, especially in morphodynamically complex river systems.

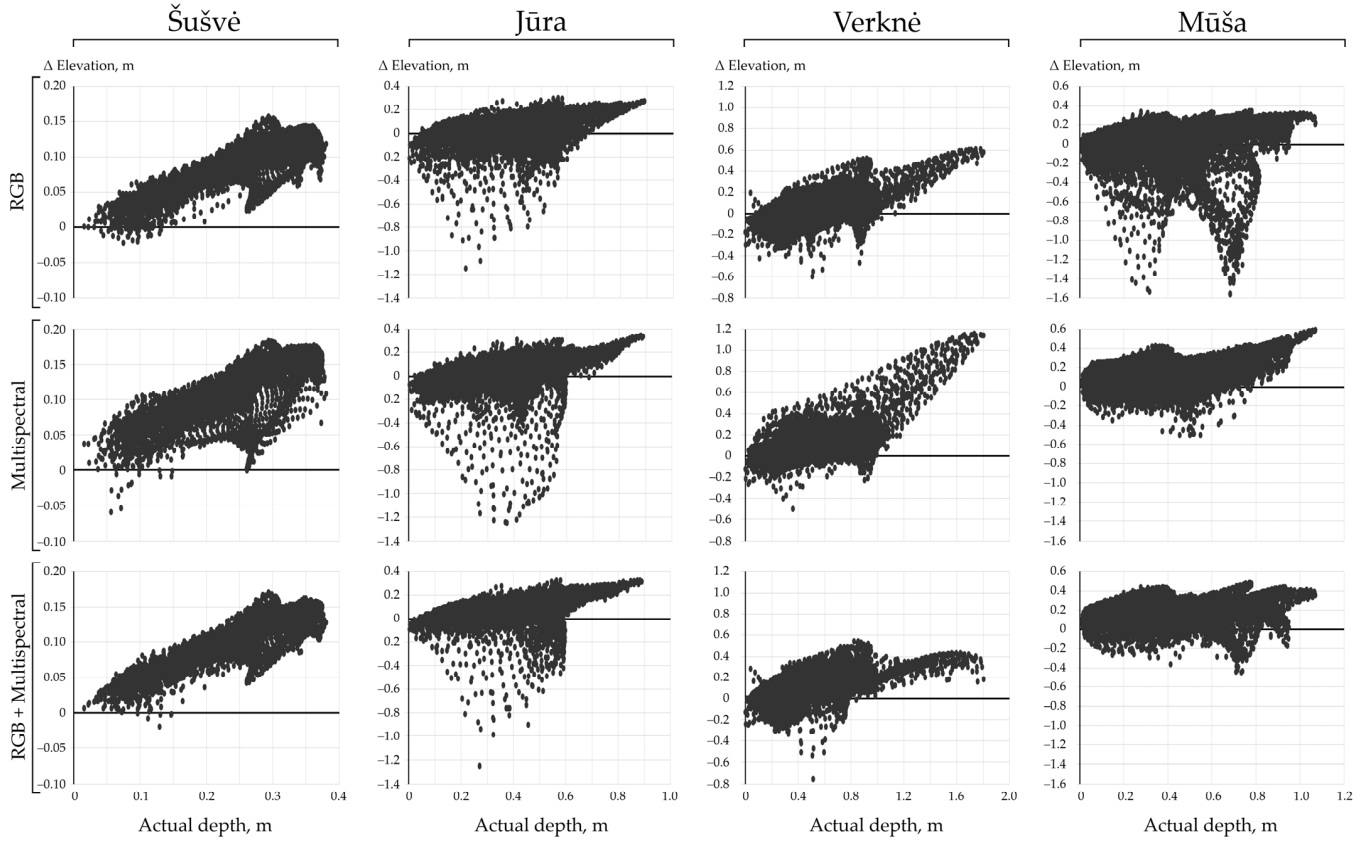

Figure 4. The relation of differences between photogrammetry-based DEM (RGB, multispectral, and RGB with multispectral imagery) and observed elevation with the actual depth in the Šušvė, Jūra, Verknė, and Mūša rivers.

3.2. Performance of the Hydrodynamic Modelling

For each selected case study, HEC-RAS 2D hydrodynamic models were developed to simulate flow conditions at the measured discharges and to represent flow structure based on the observed DEM and additional photogrammetry-based DEMs. The models were designed to simulate flow conditions representative of summer low-flow periods, as these are most critical for future hydrological and ecological impact assessments, particularly due to their influence on habitat availability and water quality under reduced discharges. The main calibration and validation metrics of the HEC-RAS 2D hydrodynamic models are listed for each selected river section (Table 3). Calibration focused on comparing the average

water surface elevation and velocity with measured field data within each river section under steady flow conditions. The results show a high level of agreement between measured and simulated values at all sites. The absolute differences in water surface elevation along the stretches were minimal, ranging from 0.001 to 0.004 m during calibration and from 0.004 to 0.008 m during validation. These deviations are well within the accepted range for the calibration of 2D hydraulic models and reflect accurate geometric and hydraulic input data. For velocity, minor differences were found between measured and simulated values. In the simplest case study of the Šušvė River, the difference between measured and simulated average flow velocity was only 0.003 m/s, while in a morphologically diverse river such as the Jūra, this difference increased to 0.02 m/s. The Verknė River simulation showed a slight underestimation of average flow velocity during calibration (0.422 m/s measured vs. 0.406 m/s simulated), while in the Mūša River, both measured and simulated average velocities were even lower, at 0.296 and 0.284 m/s, respectively. The overall differences in simulated average flow velocity did not exceed 5% of the measured values, indicating a good representation of hydrodynamic conditions. These small deviations can be attributed to local microtopographic variations, vegetation-related unevenness, or slight inaccuracies in point velocity measurements, which are inherently difficult to capture under shallow and heterogeneous conditions. This was confirmed by the RMSE, which showed a decrease in accuracy with increasing complexity of the stretch: Šušvė, with a relatively clean riverbed, showed an RMSE of only 0.052 m/s, while stretches with diverse morphology, boulders, and dense aquatic vegetation resulted in an RMSE of 0.196 m/s (Table 3). Model validation was carried out under higher discharge scenarios, which are also typical for the upper boundary of summer low flow or close to the annual average discharge. The discharge values for validation ranged from 2.20 m^3/s in the Šušvė to 4.89 m^3/s in the Verknė. The simulated water levels during validation closely matched the observed data, confirming the stability and transferability of the models' performance over a range of discharge conditions. Overall, the hydrodynamic models demonstrated robust calibration and validation performance in all four selected river stretches. The strong agreement between simulated and observed measurements confirms their suitability for simulation based on UAV-derived DEMs, especially when enhanced by multispectral fusion, to support accurate hydraulic modelling. This provides the basis for subsequent analyses of discharge structure assessment, habitat mapping, and ecological risk assessment under different discharge conditions.

Table 3. Calibration and validation metrics for the case study river stretches.

Metric		Šušvė	Jūra	Verknė	Mūša
Calibration discharge (m^3/s)		0.70	1.01	2.11	0.50
Average water surface elevation of the stretch (m, a.s.l.)	Measured Simulated	25.854 25.857	38.243 38.244	49.098 49.099	38.031 38.027
Average flow velocity at the points (m/s)	Measured Simulated	0.293 0.296	0.392 0.372	0.422 0.406	0.296 0.284
RMSE of flow velocity at the points (m/s)	Simulated	0.052	0.166	0.162	0.196
Validation discharge (m^3/s)		2.20	3.24	4.89	2.37
Average water surface elevation of the stretch (m, a.s.l.)	Measured Simulated	26.093 26.097	38.400 38.405	49.267 49.259	38.193 38.199

3.3. Changes in Hydrodynamics

The simulated flow velocity fields for each river stretch under four different topographic inputs (observed DEM and photogrammetry-based DEMs generated using RGB, multispectral, and fused RGB and multispectral images) are shown in Figures 5–8. The comparison demonstrates how the quality of photogrammetry-based topographic input

affects hydraulic properties, particularly flow velocity fields and magnitude distribution. The Šušvė River stretch represented the optimal scenario for UAV imagery-based hydrodynamic modelling, as it features homogeneous channel morphology and lacks aquatic vegetation or large bedforms. All DEM sources produced comparable velocity fields, with only minor differences in size and structure (Figure 5) compared to the reference simulation based on observed topography (Figure 5a). In the pure RGB simulation, velocities in the center of the channel were slightly overestimated, with increased velocities towards the banks, likely due to overestimated bed elevations in deeper zones (Figure 5b). In contrast, the pure multispectral DEM resulted in accelerated flow velocity zones in the center of the channel, possibly due to vertical distortion in deeper areas, as this analysis found that multispectral images exhibited more pronounced distortions with increasing river depth (Figure 5c). However, the simulation based on the combination of RGB and multispectral data reproduced the reference case more accurately, especially in representing the uniform acceleration of the central channel, missing some relatively faster zones but maintaining the marginal recirculation zones in the cross-sectional profile (Figure 5d). This river stretch served as a benchmark and confirmed the high suitability of photogrammetric methods under optically favorable and near-ideal natural conditions, with the absence of environmental obstacles that could cause hydrodynamic distortions.

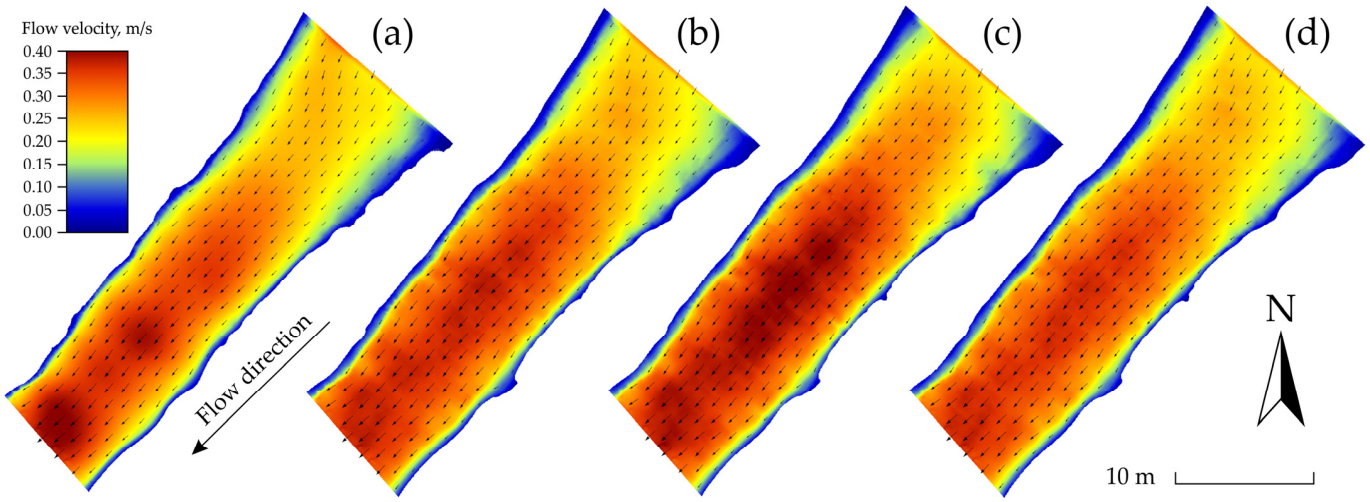

Figure 5. Simulated flow velocity at 0.70 m^3/s in the Šušvė River stretch using a DEM based on (**a**) real observations and photogrammetry-based DEMs using (**b**) RGB, (**c**) multispectral, and (**d**) RGB with multispectral images.

In the Jūra River, greater spatial morphological variability and the presence of boulders led to clearer differences between the various topographic DEM input simulations (Figure 6). The DEM derived from the RGB produced higher velocity areas near constrictions in the center of the river stretch and the downstream bend, exceeding the values observed in the reference case (Figure 6b). The multispectral simulation reduced the velocity peaks at the center of the stretch compared to RGB, although it significantly overestimated flow velocities at the end of the simulated river stretch. This pattern expanded the faster flow area and distributed it more evenly across the river, whereas in the reference simulation, these fast flows were observed closer to the right bank. The RGB and multispectral fusion provided the best agreement with the observed simulation by capturing both the relative magnitude and the pattern with the lowest distortions compared to the other spectra. This combination preserved the acceleration zones while avoiding unrealistic extreme values. These results highlight the added value of multispectral imagery in reducing

optical misinterpretations caused by separate RGB or multispectral data, especially in morphologically complex areas.

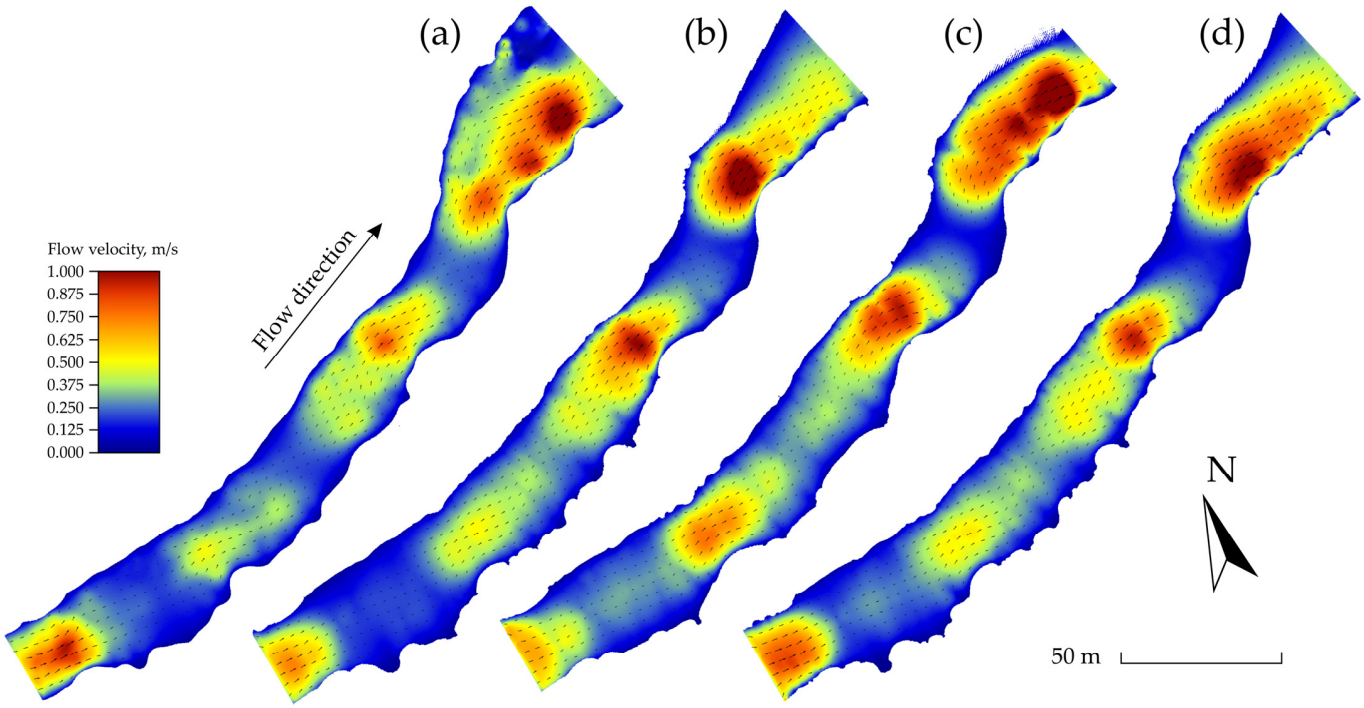

Figure 6. Simulated flow velocity at 1.01 m^3/s in the Jūra River stretch using a DEM based on (**a**) real observations and photogrammetry-based DEMs using (**b**) RGB, (**c**) multispectral, and (**d**) RGB with multispectral images.

The section of the Verknė River is characterized by dense aquatic vegetation, which significantly affected the accuracy of the photogrammetry-based DEM and, consequently, the subsequent hydrodynamic results (Figure 7). All three DEMs derived from photogrammetry similarly reproduced the general flow structure observed in the reference simulation, but with varying degrees of magnitude distortion along the river stretch (Figure 7b–d). None of these DEM-based simulations accurately reproduced the shallow area with a relatively steep slope in the middle of the selected segment, where a natural sill was visible in the reference simulation with flow velocities above 1 m/s. Simulations based on photogrammetry-derived DEMs underestimated the local acceleration zone at that sill. However, the deeper basin with decelerated flow after the sill was best represented in the combined RGB and multispectral simulation, indicating improved vertical accuracy due to sensor fusion (Figure 7d). All cases represented the zone of increased flow at the end of the stretch well, but again, the DEM based on the combination of RGB and multispectral images matched the reference simulation more closely. This case emphasizes the challenges posed by vegetation interference, where results are similar between various combinations but highlight the crucial role of applying multiple spectra in transition areas between different morphological forms, such as rapid and pool systems.

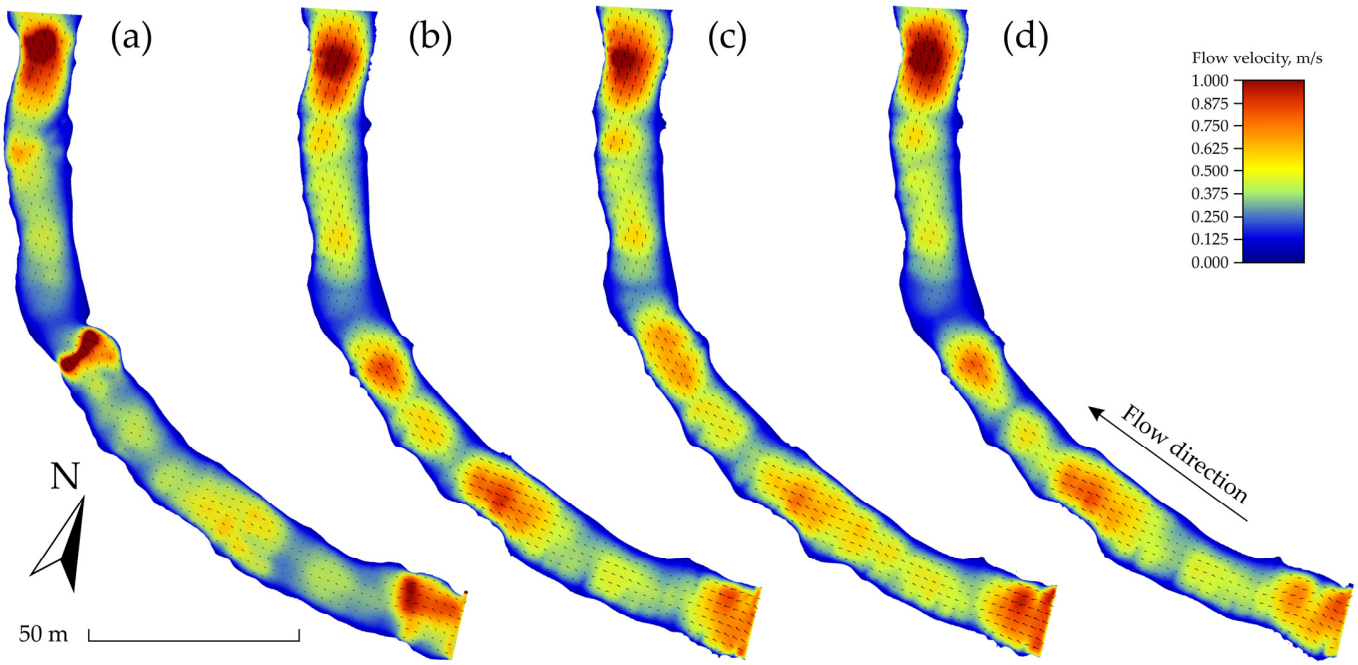

Figure 7. Simulated flow velocity at 2.11 m^3/s in the Verknė River stretch using a DEM based on (**a**) real observations and photogrammetry-based DEMs using (**b**) RGB, (**c**) multispectral, and (**d**) RGB with multispectral images.

The Mūša River showed the largest discrepancy in flow fields between the photogrammetry-based and observation-based simulations among the analyzed river stretches, due to its more diverse morphology and the presence of both vegetation and boulder features (Figure 8). The hydrodynamic simulation using the RGB-based DEM accurately captured the faster flow area at the beginning of the river stretch and the complex patterns in the middle and lower reaches (Figure 8b). However, flow velocity magnitudes were underestimated in the middle part and overestimated in the rapid part at the end of the stretch. The multispectral DEM reduced some of these hydrodynamic discrepancies and produced smoother velocity gradients in the shallower depth zones (Figure 8c). In contrast to the Verknė River, in the Mūša River, the use of only the multispectral image-based DEM captured the sill in the middle of the stretch, and a flow acceleration close to the real condition was simulated there. The combination of RGB and multispectral imagery provided balance and good overall agreement with the observation-based simulation (Figure 8d). The accurate representation of natural flow patterns in the downstream section, where the slope increases and a rapid zone occurs, demonstrates the advantages of fusing different spectra, despite the smoothing of flow changes in other transitional areas. This supports the conclusion that spectral fusion improves the consistency of the DEM, especially in challenging optical environments with aquatic vegetation and boulders. At the same time, the application of each spectrum separately highlights certain essential zones but distorts other parts of the river stretch, suggesting the need for approaches that determine the hierarchy and priority of one spectrum over another.

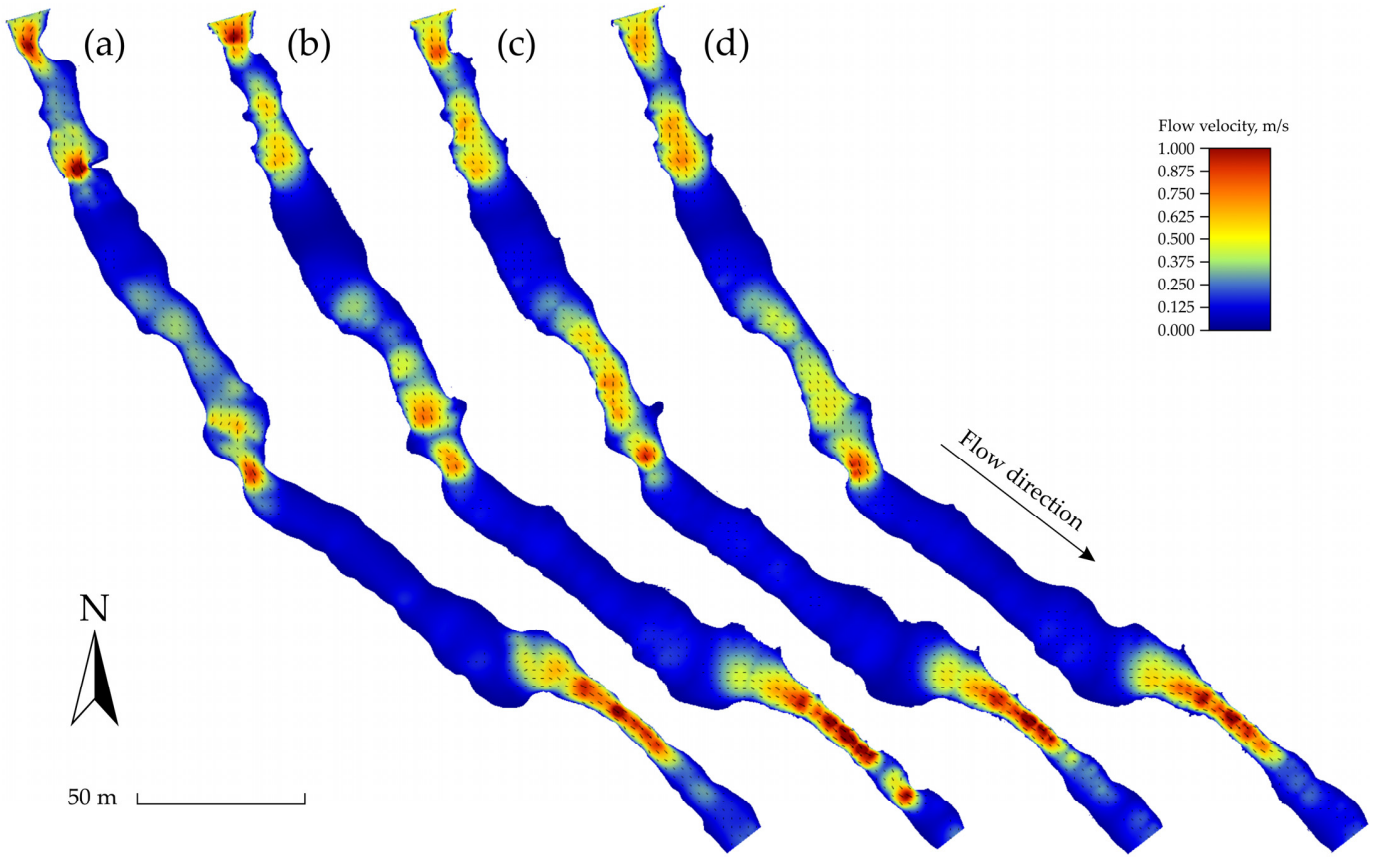

Figure 8. Simulated flow velocity at 0.5 m^3/s in the Mūša River stretch using a DEM based on (**a**) real observations and photogrammetry-based DEMs applying (**b**) RGB, (**c**) multispectral, and (**d**) RGB with multispectral images.

Overall, the comparative analysis of simulated flow fields and velocities in the four river stretches showed a clear dependence of the hydrodynamic model's accuracy on both channel complexity and the spectral composition of the photogrammetric input data. The closest agreement with observed simulations was consistently achieved using a combination of RGB and multispectral imagery, regardless of river type. This fusion approach effectively mitigated both overestimation (typically observed with RGB-only data) and over-smoothing (common with multispectral-only DEMs), particularly in deeper and vegetated sections. The most accurate hydrodynamic reconstruction was found in the Šušvė River, where minimal vegetation and uniform morphology provided ideal conditions for photogrammetric surface reconstruction. However, in the Verknė and Mūša rivers, where submerged vegetation dominated, larger discrepancies occurred. These were particularly pronounced in pure RGB simulations, which tended to misrepresent both relative depth and flow gradients. In such cases, RGB and multispectral fusion significantly improved the identification of high-velocity cores, despite the smoothing effect from the multispectral component. The Jūra River, with its clean channel but abundant boulders, provided a transitional case that illustrated the sensitivity of UAV-derived DEMs to substrate texture and optical reflectance properties. In summary, although photogrammetric approaches have great potential to support hydrodynamic simulations, their performance varies depending on local river conditions and must be adjusted according to planned applications. Sensor fusion strategies significantly improve the reliability of flow modelling, especially in optically complex or vegetated environments. These results emphasize the importance of tailoring UAV data acquisition strategies to site-specific characteristics when applying structure-from-motion techniques for hydrodynamic model inputs.

The relationships between simulated flow velocities derived from measurement-based digital elevation models (DEMs) and those from photogrammetry-based DEMs were analyzed for all selected case studies in this study (Figure 9). Among the rivers, Šušvė showed the strongest relation across all three images, with coefficients of determination (R^2) above 0.85 and a maximum value of 0.91 for the combined RGB and multispectral imagery. Even the RGB-based simulation showed a strong R^2 of 0.90. This close relation was attributed to the relative simplicity of the riverbed, as the absence of vegetation and boulders resulted in less variation in DEM elevation and the corresponding velocities. In contrast, the Jūra and Verknė rivers displayed greater scatter and significantly lower R^2 values, especially for pure RGB data. These rivers are characterized by complex morphological features, including numerous boulders in the Jūra and dense instream vegetation in the Verknė, which increase riverbed roughness and the spatial heterogeneity of flow resistance. The photogrammetry-based DEMs in these areas likely misrepresented some submerged or semi-submerged obstacles, leading to discrepancies in hydrodynamic simulations compared to those based on measurement-derived DEMs. Notably, the combined RGB and multispectral imagery improved model performance in all rivers, especially in the Jūra, where R^2 increased from 0.52 (RGB only) and 0.68 (multispectral only) to 0.73 with the combined imagery dataset. The advantages of fusing RGB and multispectral images were confirmed by flow velocity RMSE and MAE, which showed reduced errors when combining the spectra (Table 4). This suggests that multispectral data enhances the delineation of vegetated zones and submerged structures, thereby improving the visualization of riverbed features and flow paths. The Mūša River case showed intermediate behavior with noticeable relations for all applied spectra. There, the coefficient of determination for the relationship between photogrammetric input-based hydrodynamic simulations and observation-based simulations ranged from 0.66 to 0.77 (Figure 8). The presence of moderate vegetation and occasional boulders caused some deviations, but the fusion of RGB and multispectral images reduced the scatter of the results and increased the agreement between photogrammetry-based and measurement-based hydrodynamic simulations.

Table 4. Summary of flow velocity RMSE (m/s) and MAE (m/s) for each spectrum-based DEM simulation compared to observation-based hydrodynamic simulation at selected river sites.

Spectrum	Metric	Šušvė	Jūra	Verknė	Mūša
RGB	RMSE	0.031	0.150	0.164	0.128
	MAE	0.025	0.106	0.110	0.082
Multispectral	RMSE	0.045	0.138	0.158	0.120
	MAE	0.039	0.106	0.114	0.075
Multispectral+RGB	RMSE	0.027	0.112	0.152	0.099
	MAE	0.021	0.084	0.101	0.063

These results suggest that the accuracy of velocity simulations using photogrammetry-derived DEMs is strongly influenced by riverbed complexity, with vegetation cover and the presence of boulders as important factors. Furthermore, combining RGB and multispectral imagery improved the model's predictive capacity in all case studies except the simplest, where RGB-only and combined spectra performed similarly. This demonstrates the value of combined imagery for hydrodynamic modelling in homogenous stretches and its potential for morphologically diverse river systems.

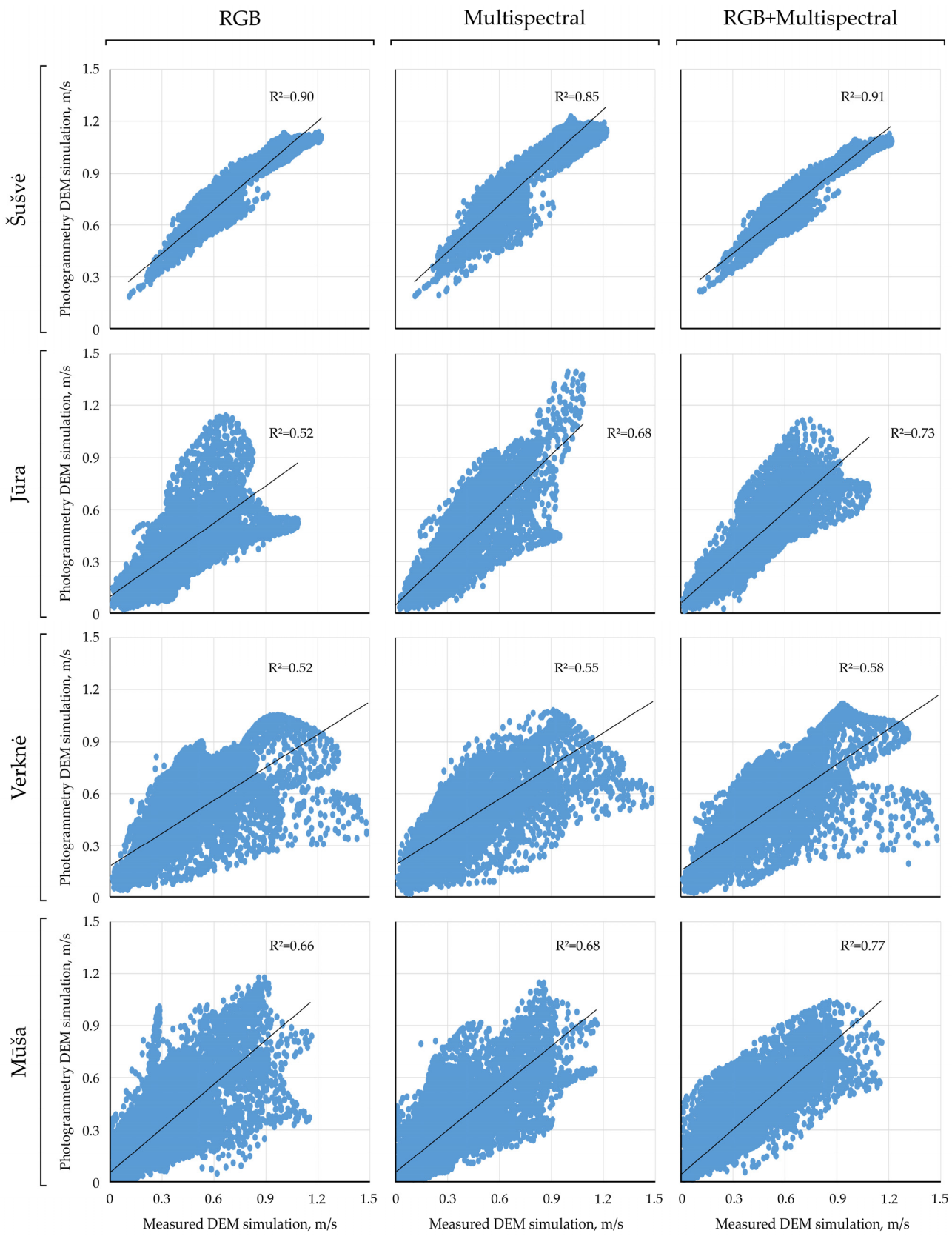

Figure 9. Relation between simulated flow velocity using a measurement-based DEM (X axis) and photogrammetry-based DEMs (Y axis) for RGB, multispectral, and RGB with multispectral imagery in the Šušvė, Jūra, Verknė, and Mūša rivers at the calibration discharge.

4. Discussion and Conclusions

Unmanned Aerial Vehicle (UAV) photogrammetry has become a valuable tool for capturing fine-scale topographic data in riverine environments. This study systematically evaluated the performance of UAV-derived Digital Elevation Models (DEMs) using RGB, multispectral, and combined imagery in four lowland rivers with diverse morphological characteristics. The results clearly show that UAV photogrammetry, particularly when integrating RGB and multispectral data, can provide elevation inputs of sufficient quality to support two-dimensional (2D) hydrodynamic modelling across varied conditions.

The improved performance of fused RGB–multispectral DEMs can be attributed to the complementary strengths of the two sensor types. RGB imagery provides fine spatial detail and sharp textural contrast in shallow, optically clear areas, while multispectral imagery improves feature stability under variable illumination and vegetation cover. When processed together, the Structure-from-Motion algorithm benefits from enhanced key point robustness, reducing local anomalies and preserving relative topographic gradients critical for hydrodynamic simulations. The UAV-derived DEMs showed consistent spatial patterns of depth-dependent elevation errors, particularly in flooded or vegetated sections. In all case study rivers, photogrammetric reconstructions generally overestimated bed elevations, leading to underestimated water depths. This effect was more pronounced in deeper sections and in areas with aquatic vegetation or boulders. RGB imagery provided finer spatial resolution and the lowest mean vertical deviation compared to field data but was more susceptible to reflectance distortions and local anomalies. In contrast, multispectral imagery showed more spatially consistent results but tended to systematically overestimate riverbed elevation due to increased depth and smoothing effects. These findings are consistent with previous studies that identify refraction, turbidity, and vegetation interference as major sources of vertical error in UAV-based bathymetry [4,11,16,28].

Importantly, combining RGB and multispectral imagery datasets consistently improved elevation estimates. The combined imagery DEMs reduced spatial noise, mitigated extreme outliers, and provided more stable surface reconstructions across different river morphologies. These findings align with UAV-LiDAR comparison studies, which also emphasize that fusing different input data enhances terrain model accuracy [29,30]. By leveraging the high-resolution spatial detail of RGB and the spectral robustness of multispectral sensors, fusion strategies offer a practical means to overcome individual limitations and enhance data reliability. Similar conclusions have been drawn by Kozmus Trajkovski et al. [31], who highlighted the effectiveness of combined imagery in improving DEMs for aquatic environments.

Bed texture plays a critical role in determining the reliability of through-water photogrammetry, alongside vegetation cover and channel morphology. Gravel- and boulder-dominated reaches (e.g., the Jūra River) exhibited relatively stable elevation patterns, whereas sand-dominated or mixed-bed reaches showed greater scatter in photogrammetry-derived elevation differences. This increased variability is likely related to short-term bedform migration or surface reworking of fine sediments occurring between UAV image acquisition and field surveys. Similar behavior has been reported in controlled and field-based experiments by Zhang et al. [32,33], who demonstrated that fine sediment mobility can introduce elevation noise independent of optical refraction effects. The depth-dependent scatter observed in this study, particularly in shallow sandy sections, is consistent with these findings and indicates that bed texture and sediment dynamics represent an additional source of uncertainty in UAV-based bathymetric reconstruction. From a mechanistic perspective, the depth-related elevation biases observed in this study are primarily due to optical distortions caused by light refraction, water turbidity, surface glare, and vegetation occlusion. RGB imagery performs well in shallow, clear waters but is

less effective in turbid or vegetated conditions. Multispectral sensors, although more stable across varying illumination and reflectance conditions, often smooth fine topographic detail and produce positive elevation biases. The spectral fusion approach effectively balances these tendencies, generating DEMs that retain sufficient morphological detail while maintaining consistency across complex channel sections.

The implications for hydrodynamic modelling are considerable. Hydrodynamic simulations using DEMs generated by RGB and multispectral fusion produced the closest agreement with simulations based on field observations across all rivers, including those with complex morphology and diverse ecology. Notably, the Šušvė River, characterized by minimal vegetation and simple channel geometry, exhibits the highest determination coefficient ($R^2 > 0.90$) between observed and simulated velocities, regardless of the photogrammetric input. Conversely, the Verknė and Mūša rivers, characterized by dense vegetation and coarse beds, posed greater challenges for photogrammetric accuracy. In these rivers, the performance of pure RGB or multispectral DEMs declined, whereas fusion-based DEMs still provided acceptable predictive capacity. These results highlight that a lower average vertical error does not necessarily ensure better hydraulic model performance. Localized elevation anomalies, particularly those affecting flow constriction zones or depth gradients, can disproportionately distort simulated flow fields [34]. Based on the results of this study, UAV-based photogrammetry is the most suitable for hydrodynamic modelling when:

- River depths are shallow (<1 m) and flow conditions are stable;
- Vegetation cover is limited or can be partially resolved using multispectral imagery;
- Relative flow patterns and velocity distributions are more important than absolute flow velocity or depth accuracy.

Overall, the results support the conclusion that fused UAV-derived DEMs are a reliable input for 2D hydraulic modelling at a certain level of accuracy, particularly where relative hydrodynamic characteristics are of primary interest. In morphodynamically complex or densely vegetated rivers, RGB and multispectral fusion during the photogrammetric generation of DEM had its advantage in model robustness but does not fully eliminate depth-related bias. Despite moderate vertical deviations (typically 0.10–0.25 m), the simulated velocity fields maintained high relative spatial coherence with field measurements. This finding is consistent with previous studies that demonstrate improved hydraulic prediction accuracy using SfM-based terrain models in heterogeneous river environments [14,15,35,36].

The broader applicability of UAV photogrammetry is well established in scientific studies. Chandler et al. [37] and Rock et al. [38] demonstrated its early use in monitoring fine-scale morphological changes. More recent studies [6,7,39] have shown its relevance for hydraulic modelling, particularly in clear, shallow, or remote environments. The integration of UAV photogrammetry with other data sources (e.g., radar or LiDAR) has also been shown to improve elevation fidelity in challenging terrains [40,41]. This study contributes to the field by extending these findings to Central and Eastern European lowland rivers, providing region-specific insights and further validating the value of different spectral data fusion for bathymetric reconstruction.

While the results are promising, some limitations must be acknowledged. The main challenge in fluvial remote sensing is the environmental conditions that significantly affect the accuracy of the results. Consequently, remote sensing methods with acceptable accuracy function only under near-ideal water visibility conditions [42]. Additionally, water causes optical refraction at the air–water interface during aerial image capture, and the absence of correction for optical refraction is a significant methodological constraint during photogrammetric reconstruction. Refraction introduces systematic vertical distortion in

image-based bathymetry, particularly as water depth increases or viewing angles deviate from nadir [43,44]. In our study, no correction approach, such as a water surface model or Snell's Law-based adjustments, was applied, which likely contributed to overestimated bed elevations in deeper or structurally complex sections. However, this effect was somewhat mitigated by the fact that all study reaches were shallow and fully wadable, with average depths between 0.26 and 0.47 m. Based on GNSS validation, the vertical RMSE ranged from 0.09 to 0.20 m, corresponding to approximately 30–42% of the local average water depth. These errors are consistent with previous studies using uncorrected SfM techniques in similar fluvial environments [43]. Although UAV image acquisition and field surveys were conducted within a short time window, even brief time lags may allow fine sediment movement in shallow lowland rivers, potentially contributing to elevation scatter in sand-dominated reaches. Furthermore, the hydrodynamic simulations were limited to steady-state conditions and did not account for unsteady flow dynamics, turbidity effects, or sediment transport. Dynamic vegetation conditions remain an additional challenge and warrant further investigation [45,46].

Future research should investigate the integration of refraction correction techniques, dynamic vegetation masking algorithms, and AI-based image interpretation tools to improve DEM generation and processing [17,45,47]. Combined UAV–USV workflows and multi-temporal surveys may further improve spatial resolution and reduce field effort [19]. Research into the propagation of elevation uncertainties under unsteady or morphodynamically active flow conditions could help define the operational limits of UAV-derived bathymetry. In summary, this study confirms that UAV imagery-based photogrammetry, particularly when integrating RGB and multispectral imagery, provides a viable and cost-effective alternative to traditional surveying techniques at a certain level of accuracy for supporting hydrodynamic simulations. By accounting for site-specific environmental conditions and leveraging the strengths of different sensor types, UAV-derived DEMs can support robust and spatially explicit flow modelling across a wide range of riverine environments, including those with ecological significance and management needs.

Mean flow velocity used for model calibration and validation was measured at 0.6 of the total flow depth from the water surface, a commonly accepted approximation of depth-averaged velocity in shallow, wadable streams [48] and corresponds to generally accepted standards such as ISO 748:2021 [49]. This method assumes a logarithmic vertical velocity profile and has been shown to provide reliable estimates of mean velocity under steady, low-turbulence conditions, particularly in shallow natural channels [50,51]. However, in morphologically complex channels or areas affected by strong secondary currents, vegetation drags, or pronounced bed roughness, the 0.6-depth method may introduce additional uncertainty compared to multi-point velocity integration. In this study, all investigated river stretches were shallow and fully wadeable, and velocity measurements were collected under stable flow conditions, reducing this uncertainty. As the same measurement approach was applied consistently across all sites, potential bias related to velocity sampling depth does not affect the comparative evaluation of DEM-derived hydrodynamic model performance.

The spatial resolution of the 2D computational mesh is an additional factor influencing hydrodynamic model performance. In this study, mesh sizes were chosen to balance numerical stability, computational efficiency, and the level of topographic detail represented by the input DEMs. Finer meshes improve representation of local bed features and flow constrictions but also increase sensitivity to small-scale elevation noise present in photogrammetry-derived DEMs. Coarser meshes, by contrast, smooth local irregularities but may reduce the ability to resolve localized hydraulic gradients [52,53]. To ensure a consistent comparison, identical mesh resolutions were applied to all DEM variants within

each river reach, allowing the influence of terrain input to be isolated from grid-related effects. The only exception was applied for Šušvė River, where a clean and relatively simple canal required more detailed mesh to capture even small irregularities. The results indicate that, at the selected mesh resolutions, relative flow patterns and velocity distributions remain robust, while localized deviations are primarily controlled by DEM quality rather than mesh size, consistent with findings from previous 2D flood modelling studies that highlight numerical stability and grid-independence at appropriate resolutions [54].

Although vertical DEM errors of 0.10–0.25 m may seem substantial relative to local water depth, their impact on hydrodynamic model performance depends greatly on the application scale and modelling objective. Previous studies have shown that for applications such as habitat mapping and ecohydraulic assessment, relative velocity patterns, flow structure, and the spatial distribution of hydraulic units can remain robust despite moderate bathymetry uncertainty, as interpretation often relies on spatial contrast rather than precise absolute depths [55–57]. In contrast, applications requiring high absolute depth accuracy—such as sediment transport or morphodynamic modelling—are much more sensitive to systematic elevation bias, as small geometric errors propagate into shear stress estimates and transport capacity and therefore may require refraction correction or complementary survey methods to reduce uncertainty [58].

Author Contributions: Conceptualization, V.A., K.G. and R.B.; methodology, V.A., K.G. and R.B.; software, K.G. and V.A.; validation, K.G., A.K. and D.Č.; formal analysis, K.G., V.A., D.M.-L. and D.Č.; data curation, K.G., A.K. and V.A.; writing—original draft preparation, K.G., D.M.-L. and D.Č.; writing—review and editing, D.M.-L., K.G., V.A., A.K. and R.B.; visualization, K.G. and V.A.; project administration, V.A. and R.B.; funding acquisition, R.B. All authors have read and agreed to the published version of the manuscript.

Funding: This research was funded by the Research Council of Lithuania, Agreement Number S-MIP-23-88.

Data Availability Statement: The data that support the findings of this study are available from the paper authors upon reasonable request.

Acknowledgments: This research was supported by the Research Council of Lithuania (LMTLT) under the Researcher Groups project program through the scientific study "Development of Combined Physical Behavior and Artificial Intelligence Models to Determine Hydromorphology of Rivers by Indirect Measurements (ArtHyReS)".

Conflicts of Interest: The authors declare no conflicts of interest.

References

1. Aneesh, P.C.; Thomas, R.M. Hydraulic Modeling of the Periyar River Using HEC-RAS: Unraveling Flow Dynamics. *Water Sci. Technol.* **2024**, *89*, 2676–2684. [CrossRef]
2. Pareta, K. 1D-2D Hydrodynamic and Sediment Transport Modelling Using MIKE Models. *Discov. Water* **2024**, *4*, 94. [CrossRef]
3. Vaze, J.; Teng, J.; Spencer, G. Impact of DEM Accuracy and Resolution on Topographic Indices. *Environ. Model. Softw.* **2010**, *25*, 1086–1098. [CrossRef]
4. Song, Y.; Huang, J.; Toorman, E.; Yang, G. Reconstruction of River Topography for 3D Hydrodynamic Modelling Using Surveyed Cross-Sections: An Improved Algorithm. *Water* **2020**, *12*, 3539. [CrossRef]
5. Ahmad, I.; Farooq, R.; Ashraf, M.; Waseem, M.; Shangguan, D. Improving Flood Hazard Susceptibility Assessment by Integrating Hydrodynamic Modeling with Remote Sensing and Ensemble Machine Learning. *Nat. Hazards* **2025**, *121*, 7839–7868. [CrossRef]
6. Gu, P.; Liao, A.; Liu, H.; Wu, W.; Wu, Y.; Liu, G.; Cao, J.; Wang, G.; Jiang, X.; Hu, P. River Cross-Section Measurement Using Unreviewed Aerial Vehicle with an Improved Bathymetry Instrument. *J. Hydrol.* **2023**, *624*, 129737. [CrossRef]
7. Koutalakis, P.; Zaimes, G.N. River Flow Measurements Utilizing UAV-Based Surface Velocimetry and Bathymetry Coupled with Sonar. *Hydrology* **2022**, *9*, 148. [CrossRef]
8. Villanueva, J.R.E.; Pérez-Montiel, J.I.; Nardini, A.G.C. DEM Generation Incorporating River Channels in Data-Scarce Contexts: The "Fluvial Domain Method". *Hydrology* **2025**, *12*, 33. [CrossRef]

9. Eltner, A.; Sofia, G. Structure from Motion Photogrammetric Technique. In *Developments in Earth Surface Processes*; Elsevier: Amsterdam, The Netherlands, 2020; Volume 23, pp. 1–24, ISBN 9780444641779.
10. He, J.; Lin, J.; Liao, X. Fully-Covered Bathymetry of Clear Tufa Lakes Using UAV-Acquired Overlapping Images and Neural Networks. *J. Hydrol.* **2022**, *615*, 128666. [CrossRef]
11. Eltner, A.; Hoffmeister, D.; Kaiser, A.; Karrasch, P.; Klingbeil, L.; Stöcker, C.; Rovere, A. (Eds.) *UAVs for the Environmental Sciences: Methods and Applications*; wbg Academic: Darmstadt, Germany, 2022; ISBN 9783534405909, 9783534405886.
12. Wang, E.; Li, D.; Wang, Z.; Cao, W.; Zhang, J.; Wang, J.; Zhang, H. Pixel-Level Bathymetry Mapping of Optically Shallow Water Areas by Combining Aerial RGB Video and Photogrammetry. *Geomorphology* **2024**, *449*, 109049. [CrossRef]
13. Hawker, L.P. Regional Flood Models and Digital Elevation Model (DEM) Uncertainty. Ph.D. Thesis, University of Bristol, Bristol, UK, 25 June 2019.
14. Langhammer, J.; Bernsteinová, J.; Miřijovský, J. Building a High-Precision 2D Hydrodynamic Flood Model Using UAV Photogrammetry and Sensor Network Monitoring. *Water* **2017**, *9*, 861. [CrossRef]
15. Annis, A.; Nardi, F.; Petroselli, A.; Apollonio, C.; Arcangeletti, E.; Tauro, F.; Belli, C.; Bianconi, R.; Grimaldi, S. UAV-DEMs for Small-Scale Flood Hazard Mapping. *Water* **2020**, *12*, 1717. [CrossRef]
16. Masafu, C.; Williams, R.; Shi, X.; Yuan, Q.; Trigg, M. Unpiloted Aerial Vehicle (UAV) Image Velocimetry for Validation of Two-Dimensional Hydraulic Model Simulations. *J. Hydrol.* **2022**, *612*, 128217. [CrossRef]
17. Agrafiotis, P.; Skarlatos, D.; Georgopoulos, A.; Karantzalos, K. Shallow Water Bathymetry Mapping from UAV Imagery Based on Machine Learning. *ISPRS—Int. Arch. Photogramm. Remote Sens. Spat. Inf. Sci.* **2019**, *XLII-2/W10*, 9–16. [CrossRef]
18. Agrafiotis, P.; Karantzalos, K.; Georgopoulos, A.; Skarlatos, D. Learning from Synthetic Data: Enhancing Refraction Correction Accuracy for Airborne Image-Based Bathymetric Mapping of Shallow Coastal Waters. *PFG* **2021**, *89*, 91–109. [CrossRef]
19. Tripathi, J.; Murphy, R. Using an Uncrewed Surface Vehicle to Create a Volumetric Model of Non-Navigable Rivers and Other Shallow Bodies of Water. *arXiv* **2023**. [CrossRef]
20. Smith, M.W.; Vericat, D. Evaluating Shallow-Water Bathymetry from Through-Water Terrestrial Laser Scanning under a range of Hydraulic and Pphysical Water Quality Conditions. *River Res. Apps* **2014**, *30*, 905–924. [CrossRef]
21. Kasvi, E.; Salmela, J.; Lotsari, E.; Kumpula, T.; Lane, S.N. Comparison of Remote Sensing Based Approaches for Mapping Bathymetry of Shallow, Clear Water Rivers. *Geomorphology* **2019**, *333*, 180–197. [CrossRef]
22. Frizzle, C.; Trudel, M.; Daniel, S.; Pruneau, A.; Noman, J. LiDAR Topo-bathymetry for Riverbed Elevation Assessment: A Review of Approaches and Performance for Hydrodynamic Modelling of Flood Plains. *Earth Surf. Process. Landf.* **2024**, *49*, 2585–2600. [CrossRef]
23. Fleit, G. Windowed Anisotropic Local Inverse Distance-Weighted (WALID) Interpolation Method for Riverbed Mapping. *Acta Geophys.* **2024**, *73*, 2819–2833. [CrossRef]
24. Bures, L.; Sychova, P.; Maca, P.; Roub, R.; Marval, S. River Bathymetry Model Based on Floodplain Topography. *Water* **2019**, *11*, 1287. [CrossRef]
25. Tuyet Minh, D. A Comprehensive Overview on UAV-Based Applications for Flood Management. *Meas. Sci. Technol.* **2025**, *36*, 086006. [CrossRef]
26. Gonçalves, J.A.; Meyer, M.; Bio, A. Precise Georeferencing of RGB and Multispectral Drone Images without Ground Control Points. *Int. Arch. Photogramm. Remote Sens. Spat. Inf. Sci.* **2025**, *XLVIII-2/W11-2025*, 103–109. [CrossRef]
27. Kujawa, P.; Wajs, J.; Pleśniak, K. The Approach to UAV Image Acquisition and Processing for Very Shallow Water Mapping. *Int. J. Appl. Earth Obs. Geoinf* **2025**, *141*, 104604. [CrossRef]
28. Elias, M.; Isfort, S.; Eltner, A.; Maas, H.-G. UAS Photogrammetry for Precise Digital Elevation Models of Complex Topography: A Strategy Guide. *ISPRS Ann. Photogramm. Remote Sens. Spat. Inf. Sci.* **2024**, *X-2–2024*, 57–64. [CrossRef]
29. Polat, N.; Uysal, M. An Experimental Analysis of Digital Elevation Models Generated with Lidar Data and UAV Photogrammetry. *J. Indian Soc. Remote Sens.* **2018**, *46*, 1135–1142. [CrossRef]
30. Escobar Villanueva, J.R.; Iglesias Martínez, L.; Pérez Montiel, J.I. DEM Generation from Fixed-Wing UAV Imaging and LiDAR-Derived Ground Control Points for Flood Estimations. *Sensors* **2019**, *19*, 3205. [CrossRef]
31. Kozmus Trajkovski, K.; Grigillo, D.; Petrovič, D. Optimization of UAV Flight Missions in Steep Terrain. *Remote Sens.* **2020**, *12*, 1293. [CrossRef]
32. Zhang, C.; Sun, A.; Hassan, M.A.; Qin, C. Assessing Through-Water Structure-from-Motion Photogrammetry in Gravel-Bed Rivers under Controlled Conditions. *Remote Sens.* **2022**, *14*, 5351. [CrossRef]
33. Zhang, C.; Li, W.; Hassan, M.A. Can Through-Water Structure-from-Motion Photogrammetry Characterize Topographic Statistics of Gravel-Bed Surfaces? *Geomorphology* **2025**, *491*, 110045. [CrossRef]
34. Veregin, H. The Effects of Vertical Error in Digital Elevation Models on the Determination of Flow-Path Direction. *Cartogr. Geogr. Inf. Syst.* **1997**, *24*, 67–79. [CrossRef]
35. Javernick, L.; Hicks, D.M.; Measures, R.; Caruso, B.; Brasington, J. Numerical Modelling of Braided Rivers with Structure-from-Motion-Derived Terrain Models. *River Res. Appl.* **2016**, *32*, 1071–1081. [CrossRef]

36. Jiménez-Jiménez, S.I.; Ojeda-Bustamante, W.; Marcial-Pablo, M.; Enciso, J. Digital Terrain Models Generated with Low-Cost UAV Photogrammetry: Methodology and Accuracy. *ISPRS Int. J. Geo-Inf.* **2021**, *10*, 285. [CrossRef]
37. Chandler, J.; Ashmore, P.; Paola, C.; Gooch, M.; Varkaris, F. Monitoring River-Channel Change Using Terrestrial Oblique Digital Imagery and Automated Digital Photogrammetry. *Ann. Assoc. Am. Geogr.* **2002**, *92*, 631–644. [CrossRef]
38. Rock, G.; Ries, J.B.; Udelhoven, T. Sensitivity Analysis of UAV-Photogrammetry for Creating Digital Elevation Models (DEM). *Int. Arch. Photogramm. Remote Sens. Spat. Inf. Sci.* **2012**, *XXXVIII-1/C22*, 69–73. [CrossRef]
39. Coveney, S.; Roberts, K. Lightweight UAV Digital Elevation Models and Orthoimagery for Environmental Applications: Data Accuracy Evaluation and Potential for River Flood Risk Modelling. *Int. J. Remote Sens.* **2017**, *38*, 3159–3180. [CrossRef]
40. Leon, J.X.; Phinn, S.R.; Hamylton, S.; Saunders, M.I. Filling the 'White Ribbon'—A Multisource Seamless Digital Elevation Model for Lizard Island, Northern Great Barrier Reef. *Int. J. Remote Sens.* **2013**, *34*, 6337–6354. [CrossRef]
41. Bures, L.; Roub, R.; Sychova, P.; Gdulova, K.; Doubalova, J. Comparison of Bathymetric Data Sources Used in Hydraulic Modelling of Floods. *J. Flood Risk Manag.* **2019**, *12*, e12495. [CrossRef]
42. Dietrich, J.T. Bathymetric Structure-from-Motion: Extracting Shallow Stream Bathymetry from Multi-view Stereo Photogrammetry. *Earth Surf. Process. Landf.* **2017**, *42*, 355–364. [CrossRef]
43. Woodget, A.S.; Dietrich, J.T.; Wilson, R.T. Quantifying Below-Water Fluvial Geomorphic Change: The Implications of Refraction Correction, Water Surface Elevations, and Spatially Variable Error. *Remote Sens.* **2019**, *11*, 2415. [CrossRef]
44. Woodget, A.S.; Carbonneau, P.E.; Visser, F.; Maddock, I.P. Quantifying Submerged Fluvial Topography Using Hyperspatial Resolution UAS Imagery and Structure from Motion Photogrammetry. *Earth Surf. Process. Landf.* **2015**, *40*, 47–64. [CrossRef]
45. Liu, D.; Valyrakis, M.; Williams, R. Flow Hydrodynamics across Open Channel Flows with Riparian Zones: Implications for Riverbank Stability. *Water* **2017**, *9*, 720. [CrossRef]
46. Ettritch, G.; Hardy, A.; Bojang, L.; Cross, D.; Bunting, P.; Brewer, P. Enhancing Digital Elevation Models for Hydraulic Modelling Using Flood Frequency Detection. *Remote Sens. Environ.* **2018**, *217*, 506–522. [CrossRef]
47. Kazanskiy, N.; Khabibullin, R.; Nikonorov, A.; Khonina, S. A Comprehensive Review of Remote Sensing and Artificial Intelligence Integration: Advances, Applications, and Challenges. *Sensors* **2025**, *25*, 5965. [CrossRef]
48. Rantz, S.E. *Measurement and Computation of Streamflow: Volume 1. Measurement of Stage and Discharge*; USGS: Washington, DC, USA, 1982; pp. 1–284. [CrossRef]
49. *ISO 748:2021*; Hydrometry—Measurement of Liquid Flow in Open Channels—Velocity Area Methods Using Point Velocity Measurements. International Organization for Standardization: Geneva, Switzerland, 2021. Available online: https://www.iso.org/standard/72754.html (accessed on 15 December 2025).
50. Davids, J.C.; Rutten, M.M.; Pandey, A.; Devkota, N.; Van Oyen, W.D.; Prajapati, R.; Van De Giesen, N. Citizen Science Flow—An Assessment of Simple Streamflow Measurement Methods. *Hydrol. Earth Syst. Sci.* **2019**, *23*, 1045–1065. [CrossRef]
51. Gordon, N.D.; McMahon, T.A.; Finlayson, B.L.; Gippel, C.J.; Nathan, R.J. *Stream Hydrology: An Introduction for Ecologists*, 2nd ed.; reprinted; Wiley: Chichester, UK, 2006; ISBN 9780470843581.
52. Horritt, M.S.; Bates, P.D. Effects of Spatial Resolution on a Raster Based Model of Flood Flow. *J. Hydrol.* **2001**, *253*, 239–249. [CrossRef]
53. Cook, A.; Merwade, V. Effect of Topographic Data, Geometric Configuration and Modeling Approach on Flood Inundation Mapping. *J. Hydrol.* **2009**, *377*, 131–142. [CrossRef]
54. Bates, P.D.; Horritt, M.S.; Fewtrell, T.J. A Simple Inertial Formulation of the Shallow Water Equations for Efficient Two-Dimensional Flood Inundation Modelling. *J. Hydrol.* **2010**, *387*, 33–45. [CrossRef]
55. Pasternack, G.B.; Gilbert, A.T.; Wheaton, J.M.; Buckland, E.M. Error Propagation for Velocity and Shear Stress Prediction Using 2D Models for Environmental Management. *J. Hydrol.* **2006**, *328*, 227–241. [CrossRef]
56. McKean, J.; Tonina, D.; Bohn, C.; Wright, C.W. Effects of Bathymetric Lidar Errors on Flow Properties Predicted with a Multi-Dimensional Hydraulic Model: Lidar Bathymetry and Hydraulic Models. *J. Geophys. Res. Earth Surf.* **2014**, *119*, 644–664. [CrossRef]
57. Benjankar, R.; Tonina, D.; McKean, J. One-dimensional and Two-dimensional Hydrodynamic Modeling Derived Flow Properties: Impacts on Aquatic Habitat Quality Predictions. *Earth Surf. Process. Landf.* **2015**, *40*, 340–356. [CrossRef]
58. Siedersleben, J.; Jocham, S.; Aufleger, M.; Klar, R. Morphodynamic Modelling with Uncertain Geometry Input. *Water* **2021**, *13*, 2248. [CrossRef]